Accepted Manuscript

Diffusion-reaction studies in low permeability shale using X-ray radiography with cesium

Diana B. Loomer, Lisa Scott, Tom A. Al, K. Ulrich Mayer, Sergio Bea

PII: S0883-2927(13)00241-2
DOI: http://dx.doi.org/10.1016/j.apgeochem.2013.09.019
Reference: AG 3120

To appear in: *Applied Geochemistry*

Received Date: 14 May 2013
Accepted Date: 26 September 2013

Please cite this article as: Loomer, D.B., Scott, L., Al, T.A., Ulrich Mayer, K., Bea, S., Diffusion-reaction studies in low permeability shale using X-ray radiography with cesium, *Applied Geochemistry* (2013), doi: http://dx.doi.org/10.1016/j.apgeochem.2013.09.019

Diffusion-reaction studies in low permeability shale using X-ray radiography with cesium

Diana B. Loomer*[,a], Lisa Scott[a,1], Tom A. Al[a], K. Ulrich Mayer[b] and Sergio Bea[b,2]

[a]Department of Earth Sciences, University of New Brunswick, PO Box 4400, Fredericton, NB Canada, E3B 5A3
(dloomer@unb.ca; ph. +1-506-453-5153), (tal@unb.ca)

[b]Department of Earth, Ocean and Atmospheric Sciences, University of British Columbia 2207 Main Mall, Vancouver, BC, Canada, V6T 1Z4 (umayer@eos.ubc.ca)

*corresponding author

[1]Permanent Address: Groundwater Resources Section, Environment Canterbury, P.O. Box 345, Christchurch, 8140, New Zealand. lisa.scott@ecan.govt.nz.

[2] Permanent Address: CONICET, IHLLA-UNICEN, República de Italia 780, Azul, Buenos Aires, C.C. 47 (B7300) Argentina. sabea@faa.unicen.edu.ar.

Abstract

An X-ray radiography method for the determination of diffusion coefficients in rock has been modified to provide an estimation of diffusion-reaction parameters for the sorbing tracer, cesium (Cs^+). Cesium tracer diffusion and sorption on cation exchange sites can be monitored in intact rock samples using data extracted from radiographs to plot time-series relative-concentration profiles of Cs^+ as a function of transport distance. Cesium was found to be a very good tracer for these experiments because of the sensitivity of the X-ray attenuation measurements to Cs^+ concentration.

Reactive-transport modeling coupled with parameter estimation software was used to match experimental data and estimate pore diffusion coefficients for Cs^+ ($D_{p\text{-}Cs} = 7.6 \times 10^{-11}$ m^2/s), single-site selectivity coefficients for Cs^+ exchange (log $K_{Cs+/Na+} = 1.5$) and cation exchange capacity (CEC = 8.4 meq/100 g) for drill core samples of Queenston Formation shale, from the Michigan Basin in Ontario, Canada.

Keywords

Diffusion; Sorption; Cesium; X-ray radiography; Sedimentary rock; Nuclear waste management; Ion exchange; Reactive transport.

1. Introduction

Sedimentary rocks with low permeability and porosity are under consideration in Canada as potential host rocks for a deep geological repository for the long term containment of radioactive waste. One of the benefits of these rock types for this purpose is that advection is minimized, resulting in diffusion-dominated transport of solutes. Diffusive solute transport, coupled to ion-

exchange processes, is of interest because radionuclides such as ^{137}Cs and ^{90}Sr present in used fuel are subject to retention by ion exchange in both clay-based engineered barrier materials (e.g., bentonite) and in host rocks that have appreciable sorption capacity (van Loon et al., 2005). Quantification of transport and reaction processes affecting these solutes is, therefore, important in the assessment of material properties for a deep geologic repository. Cesium is one of the most widely studied species in sorption experiments for radioactive waste disposal (Bradbury and Baeyens, 2000; Jakob et al., 2009; Maes et al., 2008; Melkior et al., 2005; Tachi et al., 2011). Cesium is soluble and bioavailable, and its simple speciation (occurring predominantly as the monovalent cation) makes it a good tracer for diffusion-reaction experiments (Melkior et al., 2005).

Previous studies of Cs^+ transport in low permeability materials have used through-diffusion experiments (Appelo et al., 2010; Jakob et al., 2009; Melkior et al., 2005), column migration experiments coupled with reactive-transport modeling (Maes et al., 2008), and in-situ studies coupled with reactive-transport modeling (Soler et al., 2013; Wersin et al., 2008). However, waiting for experiments to reach steady state can be very time consuming with a strongly sorbing tracer (months to years; Melkior et al., 2007) and researchers have been developing methods aimed at reducing total experimental time (André et al., 2009; Okuyama et al., 2008; van Loon et al., 2009). Cormenzana et al. (2003) used an in-diffusion approach to measure Cs^+ diffusion-reaction profiles during the early, transient period of transport, but the drawback is that their technique requires destruction of the samples. An X-ray radiography method for measuring iodide diffusion described by Cavé et al. (2009) has been adapted here because Cs^+ is also well suited for X-ray detection due to its strong X-ray absorption. The radiography method is nondestructive and, when relatively high tracer concentrations are used, it

allows rapid (days to weeks) collection of diffusion-reaction data during the transient (non-steady-state) period of the experiment.

The cation exchange capacity (CEC) is an intrinsic property of a geologic material that limits sorption of cations such as Cs^+ (Melkior et al., 2005). Studies of the sorption behavior of cations commonly rely on an independent determination of CEC (Jakob et al., 2009; Maes et al., 2008; Melkior et al., 2005; Tachi et al., 2011; van Loon et al., 2009). There has been debate that CEC estimates determined on crushed rock material may overestimate sorption for intact rock. André et al (2009), Jakob et al. (2009) and Maes et al. (2008) found that there were fewer exchange sites available in intact clay rocks compared to disaggregated material. Recently, though, the general consensus has developed that, for Cs^+, sorption is equivalent for disaggregated and intact systems (Altmann et al., 2012; Soler et al., 2013; Tachi et al., 2011; van Loon et al., 2009). Techniques for determining CEC use concentrated solutions of strongly exchangeable cations such as NH_4^+, Cs^+, Ca^{2+}, Sr^{2+} or Ba^{2+} , or complexes such as cobalt hexamine, silver thiourea or nickel ethylenediamine (Ni-en) to displace all exchangeable cations from the exchange sites in batch experiments with disaggregated rock samples (Bradbury and Baeyens, 1998). For samples with very high salinity porewater, there are analytical challenges in the use of these methods because the mass of cations in the porewater overwhelms that on exchange sites. For this reason, attempts to use the Ni-en method on rock samples from the present study were unsuccessful (Koroleva et al., 2009). An alternative approach is needed for measuring CEC in high-salinity systems.

There are multiple approaches for presenting diffusion-related terms in the literature, so the following definitions are provided for clarity. The pore diffusion coefficient (D_p) is defined by $D_p = D_0 \cdot \tau$, where D_0 is the free-water diffusion coefficient and τ is the dimensionless

tortuosity factor (0 – 1). The effective diffusion coefficient (D_e) is related to the D_p by $D_e = D_p \cdot \phi$, where ϕ is porosity and the apparent diffusion coefficient (D_a) is related to the D_p by $D_a = D_p/(1+K_d \cdot \rho/\phi)$ where $\rho$and K_d are the bulk density and distribution coefficients of the porous medium, respectively.

In many previous studies of Cs^+ sorption (Aldaba et al., 2010; Cormenzana et al., 2003; Maes et al., 2008; Melkior et al., 2005, 2007) the approach has been to determine distribution coefficients (K_d) and apparent diffusion coefficients (D_a) for Cs^+. The K_d for Cs^+ sorption is known to be concentration-dependent (Bradbury and Baeyens, 2000). The D_a, being a function of K_d, is also concentration-dependent. In some cases (André et al., 2009; Okuyama et al., 2008; Tachi et al., 2011), diffusion and sorption are evaluated using effective diffusion coefficients (D_e) and K_d's; the D_e values having been obtained by through diffusion using conservative (non-reactive, non-sorbing) tracers such as HTO, and the K_d values from sorption experiments on crushed or intact samples. However, it has been shown that the K_d approach to modeling sorption is problematic having been found to be tracer-concentration and solution-composition dependant as well as varying along a diffusion path in both space and time in non-steady-state conditions (e.g. Reardon, 1981; Staunton and Roubaud, 1997; Jakob et al., 2009). It would be beneficial to use an alternative approach that allows direct quantification of D_p for reactive elements. This study employs an equilibrium thermodynamic model for ion exchange which makes use of the concentration-independent terms $D_{p\text{-}Cs}$ and CEC, as well as the concentration-sensitive selectivity coefficient for Cs^+ exchange. The objective of this work was to develop a new and rapid method for the quantification of the $D_{p\text{-}Cs}$ and the CEC for intact rock samples in high salinity systems. Data sets collected using x-ray radiography combined with reactive transport modeling were used to determine these parameters simultaneously in a time efficient

manner. Selectivity coefficients, which vary for Cs^+ depending on the sorption site considered, are available from the literature over a range of Cs^+ concentrations (Appelo et al., 2010; Bradbury and Baeyens, 2000; Liu et al., 2004; van Loon et al., 2009; Zachara et al., 2002) and the results from this work are compared in context with the findings of other researchers.

2. Materials and methods

The method is a modification of the radiographic technique that was developed for I^- diffusion measurements (Cavé et al., 2009); time series measurements of changes in X-ray absorption are used to quantify the spatial distribution of Cs^+ tracer mass during transport and reaction in low permeability, sedimentary rock. The resultant Cs^+ relative concentration profiles are fit using a reactive transport model that couples diffusion and ion exchange processes. The numerical model is used to find estimates for Cs^+ pore diffusion coefficients, Cs^+/Na^+ selectivity coefficients and CEC.

2.1. Sample preparation

A sample of red shale drill core, 76 mm in diameter, with relatively uniform porosity and diffusive properties was selected from the Queenston Formation at 468 m depth in borehole DGR3. The core was drilled as part of Ontario Power Generation's Low and Intermediate Level Deep Geological Repository Geoscientific Site Characterization at the Bruce nuclear site, Ontario. Details of the drilling, coring and the drill core preservation methods are provided in Briscoe et al. (2010) and Pinder (2009).

Samples for the Cs^+ diffusion experiments were prepared from an 18-mm thick core segment cut normal to the core axis, and then drilling six subcores (11 mm diameter) from the core segment. The subcores were orientated with the core axis normal to the bedding plane.

Three of the subcores were used to determine the diffusive transport properties of the rock using the non-sorbing I^- tracer and the other three for coupled diffusive transport with sorption using a Cs^+ tracer. Water-accessible porosity, ϕ_w, measurements (Table 1) were performed as described in Cavé et al. (2009) from off-cuts of the core segment from which the subcores were removed. Additional porosity measurements and the mineralogy of the Queenston Formation shale from related studies are included in Table 1.

2.2. Measurement of diffusion properties

The measurements were conducted with the samples mounted in diffusion cells (Fig. 1). The circumference of each subcore was brushed with a thin layer of silicone then enclosed in heat-shrink tubing (3M FP-301). Discs of felt fabric, used to prevent the formation of air pockets, and ceramic caps (11 mm diameter, 3 mm height) that act as internal standards to correct for changes in the intensity of the X-ray source over time, were positioned inside the tubing on top of the samples. There are threaded holes in the ceramic discs to allow access for solutions. Two wire alignment guides were fixed at 180° from each other along the sides of the samples. The bottoms of the samples were secured in reservoirs constructed from Delrin®. Samples used for determination of D_p for the iodide tracer ($D_{p\text{-}I}$) and for iodide-accessible porosity (ϕ) were measured in triplicate and labeled as Queenston shale A, B and C. Samples used in the Cs^+ tracer experiments were labeled as Queenston shale D, E and F.

A small amount of porewater loss may occur due to evaporation during sample preparation, and in order to ensure saturation before commencing the experiments, the reservoirs were filled with synthetic porewater (SPW; Table 2); SPW was injected into the hole in the

ceramic disc to wet the top surface. The reservoirs and the ceramic cap were sealed and the solutions were refreshed weekly over a period of seven weeks.

Diffusion tests were initiated by replacing the SPW in the bottom reservoirs with tracer solution (Fig. 1). Approximately 5 times the reservoir volume (20 mL) of 1.0 mol/L I^- or 1.0 mol/L Cs^+ tracer solution (Table 2) was flushed through the reservoirs to ensure complete replacement of the SPW with tracer solution. The tracer concentrations were selected to produce high signal-to-noise ratios in the radiographs. Reference radiographs (for background subtraction) were collected immediately after tracer addition to the reservoir. The X-ray images were collected with a Skyscan 1072 Desktop MicroCT system using 90 kV source potential, 110 μA current, 10 s exposure and 8 frame image averaging (total collection time of 80 s). A one-mm aluminum filter was used to remove low energy X-rays and the CCD detector was flat-field corrected. Radiographs were collected as 16 bit TIFF image files. Reference images were collected in triplicate for each sample to evaluate data reproducibility.

Time-series radiographs were collected using the same positioning and operating conditions as for the reference radiographs. Radiograph collection continued at intervals of one day for the first three days, increasing to every three days over a period of two weeks. The tracer solutions were refreshed every three days to maintain a constant concentration boundary condition for the experiments. The estimated decrease in Cs^+ concentration in the tracer reservoir, based on model output for the total mass of Cs^+ that diffused into the samples in three days, is 3.5%. Therefore, the assumption of constant concentration boundary conditions in these experiments is valid. The I^- diffusion experiments ended when image processing revealed that the tracer had broken through the upper end of the sample.

As a requirement for the measurement of ϕ, the samples were allowed to saturate with I^- from both ends by removing the screw in the ceramic cap and immersing them in the tracer solution. Radiographs were collected intermittently through this I^- saturation period and samples were deemed saturated when there were no detectable changes in consecutive images. All samples were stored at room temperature (23°C) in a closed container with an open dish of SPW to maintain humidity and prevent evaporative drying.

2.3. Radiograph data processing

Data are collected in the form of two-dimensional (2D) digital radiographs where the greyscale value at each pixel is a function of the X-ray intensity measured at the detector. X-ray sources are polychromatic and the measured intensity is a function of the density and atomic number of the sample material and the energy of the X-rays (Wildenschild et al., 2002), but for simplicity, the measured intensity is commonly represented by the Beer-Lambert law:

$$I = I_0 e^{-\mu d} \quad (1)$$

which treats the incident beam as a monochromatic source. In equation 1, I is the measured X-ray intensity (greyscale value); I_0 is the source X-ray intensity; μ is the X-ray attenuation coefficient; and d is the thickness of the sample. For our purposes, intensity measurements from 2D radiographs are integrated horizontally across the width of the sample, producing 1D profiles of X-ray intensity versus distance along the axis of the sample. Using an approach from Cavé et al. (2009) in which the difference in X-ray attenuation between a reference image (time = 0) and a time-series image (time = t), the attenuation due to the presence of the tracer is calculated as:

$$\Delta\mu = \mu d_{t=0} - \mu d_t = [\ln (I_{t=0}) - \ln (I_t)] \quad (2)$$

The thickness, d, of the samples is constant and can be canceled out, leaving $\Delta\mu$.

The open-source ImageJ software (Rasband, 2012) was used to analyze the radiograph data. The average greyscale intensity of the internal standard was used to correct for variability in the X-ray source. Plots of the change in X-ray attenuation ($\Delta\mu_t$) versus distance were prepared for each time step.

For the non-sorbing tracer, I^-, at each point (x) in the profile the value of $\Delta\mu$ is a function of the mass or concentration (C) of I^- in the pore fluid intersected by the X-ray beam. For reactive tracers, such as Cs^+, the value of $\Delta\mu$ is a function of the total mass in the volume intersected by the X-ray beam which includes both dissolved and adsorbed Cs^+. Relative concentration profiles for I^- were developed using:

$$\left(\frac{C}{C_0}\right)_x = \frac{(\Delta\mu_t)_x}{(\Delta\mu_{sat})_x} \tag{3}$$

where $\Delta\mu_{sat}$ is obtained from the tracer-saturated sample. This relative approach does not require knowledge of sample porosity. The $D_{p\text{-}I}$ for the non-sorbing tracer in one dimension is determined by least-squares regression fit to an analytical solution of Fick's Second Law:

$$\left(\frac{C}{C_0}\right)_x = erfc\left[\frac{x}{2\sqrt{(D_{p\text{-}I}t)}}\right] \tag{4}$$

where C is the measured concentration of the tracer at position x (m); C_0 is the constant concentration of the tracer at the influx boundary; t is the time (s) since the start of diffusion; and D_p is the pore-water diffusion coefficient (m^2/s).

Profiles of $\Delta\mu_{sat}$ are used to calculate ϕ. When the $\Delta\mu_{sat}$ data are acquired, the aqueous concentration of I^- at all locations is equal to C_0; therefore, variations in the value of $\Delta\mu$ along the

length of the sample reflect differences in ϕ. Spatially resolved values for ϕ can be determined with a calibration function that relates the mass (concentration) of I^- in a sample to $\Delta\mu$:

$$(\Phi_I)_n = \frac{(\Delta\mu_{m/\rho})_x}{m \cdot C_0} \quad (5)$$

where m is the slope of the linear calibration function. Three calibration matrices were used to develop calibration functions for the I^- and Cs^+ tracers: a glass vial, a ceramic material and natural sandstones.

Cavé et al. (2009) conducted their calibration with glass vials filled with standard solutions of varying tracer concentration. However, this approach is susceptible to systematic errors that relate to differences in X-ray beam hardening between the solution-filled calibration vials and the rock samples. The effect of beam hardening must be accounted for and this has been done empirically by calibrating with standard solutions in three different materials (Fig. 2). The use of glass vials filled with solutions as reported by Cavé et al. (2009) provides data that are subject to the least amount of beam hardening. A ceramic material (Mykroy/Mycalex®) with X-ray attenuation properties similar to calcite was machined into cylinders of the same dimensions as the rock samples (11 mm diameter) and then drilled along the cylindrical axis to create vials with equivalent volumetric porosities of 0.02, 0.05, 0.10 and 0.17. Measurements with these ceramic vials are subject to a relatively high degree of beam hardening. The third material was natural sandstone with porosities that bracket the porosity in the experimental samples (Kocurek Industries Inc.; Berea Upper Gray (0.196 porosity; Kipton, Ohio); Carbon Tan (0.129 porosity; Utah) and Crab Orchard (0.054 porosity; Tennessee)). Although the supplier provides porosity data for these sandstones, we conducted ϕ_w measurements in triplicate on off cuts from the sandstone subcores and those results were used in the calibration. The

mineralogical composition of the sandstones and their natural pore distribution result in beam hardening that is intermediate between the glass vials and the ceramic, and best represents the beam hardening encountered with the experimental samples. The calibration function from the sandstone was used for quantification of ϕ and I^- tracer concentrations in the experimental samples.

Calibrations are required for each tracer, I^- and Cs^+, but it is not possible to use sandstone for calibration with the Cs^+ solution because its sorption on the large mineral surface area leads to erroneous results. To overcome this limitation, calibrations were conducted with the Cs^+ solutions in the glass and ceramic vials, and the ratios of the I^- calibration curve for sandstone to those from the glass and ceramic vials (Fig. 2a) were used to calculate a sandstone equivalent calibration function for Cs^+ (Fig. 2b). This approach is justifiable because the differences in the slopes for the calibration curves for the glass vial, sandstones and ceramic are due to differences in the beam hardening characteristics of the materials which are constant regardless of the composition of the filling solution.

The sandstone equivalent calibration function for Cs^+ (Fig. 2b) was used to calculate porewater-equivalent, relative Cs^+ concentrations versus distance at each time step:

$$\left(\frac{C}{C_0}\right)_n = \frac{\Delta\mu_n}{m \cdot \phi_W \cdot C_0} \qquad (6)$$

The concentration profiles were scaled by the ϕ_w values from DGR3-468.02 (Table 1). They represent total concentrations because the Cs^+ mass actually resides in the porewater and on the exchange sites.

The calibration solutions were derived from a SPW matrix, replacing the NaCl in the SPW (Table 2) with NaI or CsCl salts as required. Data collection for the calibrations used identical operating conditions to those for experimental data collection. Duplicate standards and repeat radiographs were used to determine experimental precision for $\Delta\mu$.

2.4. Diffusion-reaction simulations

The multicomponent reactive transport code MIN3P-NWMO (Mayer et al., 2002; Bea et al., 2011) was used to simulate diffusive transport and ion exchange in one dimension. The parameter estimation code, PEST v.12.2 (Doherty, 2010) was used to match simulated Cs^+ concentration profiles to the experimental profiles, providing simultaneous estimates of $D_{p\text{-}Cs}$, the selectivity coefficient for Cs^+ exchange with Na^+ (log $K_{Cs+/Na+}$) and CEC for each sample. The fitting was performed with PEST in the iterative, nonlinear parameter estimation mode (a Gauss-Marquardt-Levenberg algorithm). The estimation of log $K_{Cs+/Na+}$ is based on ion exchange on a single type of surface site ($XNa + Cs^+ = XCs + Na^+$), unlike several previous studies which use 2 or 3 binding sites, (Bradbury and Baeyens, 2000; Maes et al., 2008; Steefel et al., 2003; van Loon et al., 2009).

The transport domain was divided into 40 cells along the length of a sample. To fit the experimental data to the model domain, PEST requires a corresponding data value for each cell. The data profiles consist of approximately 800 data points, each representing 1 pixel in the image. To reduce the number of data points to match the 40 cells in the model domain, polynomial curves were fit to the data using the open-source polynomial regression java applet, PolySolve Version 3.4 (Lutus, 2011). The equation for the fitted curve was then used to calculate the Cs^+ concentration at distances corresponding to the center of each cell.

Initially, material in each cell was assigned a CEC and equilibrated with SPW. The bulk dry density was 2.54 g/cm^3 and the bulk porosity used for the simulations was 0.109 (Table 1). Simulations were conducted with no advective transport (i.e., diffusion only). Prescribed constant-concentration and zero-mass-flux boundary conditions were imposed at the influx boundary and at the end of the domain, respectively. Ion activity coefficients were calculated using an ion-interaction approach (HW model, Harvie et al., 1984), as implemented by Bea et al. (2010, 2011). The Cs^+ ion interaction parameters selected for the model from various literature sources were added to the Harvie et al. (1984) virial coefficients database, and are shown in Table 3. Coefficients obtained from measurements in the NaCl-CsCl system were favored when selecting from a range of available literature values. In addition to Cs^+- Na^+ exchange, equilibrium-controlled ion-exchange reactions based on the Gaines-Thomas convention (Mayer et al., 2002) were included for the major ions in the SPW and tracer solutions (log $K_{Cation/Na+}$ = Na^+ 0.0, K^+ 0.7, Ca^{2+} 0.8, Mg^{2+} 0.6; Appelo and Postma, 1993). Within MIN3P, all exchange reactions are referenced to Na^+ and, as described in Appelo and Postma (1993), the exchange coefficients for other cation pairs are obtained by combining the appropriate Na-based reactions. Therefore, competitive exchange with other cations is implicitly accounted for in the model. During parameter estimation, the selectivity coefficients for other cations were held constant and only log $K_{Cs+/Na+}$ was optimized.

3. Results and Discussion

3.1. Iodide

The analytical solution for diffusive transport provides a very good fit to the I^- relative-concentration profiles (Fig. 3). The combined geometry of the samples and the cone-shaped X-ray beam causes some minor blurring of the signal near the influx boundary. This results in loss

of data over a 2.0-2.5 mm distance from the boundary. However, the fitting procedure relies on the whole data profile and the influence of this data gap near the boundary on the D_{p-I} determination is negligible.

The variation in the best-fit D_{p-I} value over time (Fig. 3) arises from sample heterogeneity. The mean of the best-fit D_{p-I} values then represents a bulk D_{p-I} for the sample and the standard deviation (σ) gives an indication of the variability in the sample (Table 4). The radiography data for the non-sorbing I^- tracer can also provide spatially-resolved, one-dimensional ϕ profiles (Fig. 3), which provide an indication of the variability in sample porosity. The ϕ values reported in Table 4 represent the mean ϕ from each profile. The D_{p-I} and ϕ values for samples A and B are in very good agreement, while the D_{p-I} and ϕ values for sample C are slightly lower (Table 4), the difference being due to local heterogeneity. The ratio of ϕ to ϕ_w measured for the three samples is 0.66 to 0.72, consistent with the effects of anion-exclusion reported in clay-rich media (Altmann et al., 2012; Bazer-Bachi et al., 2006; Melkior et al., 2004; Tachi et al., 2011; van Loon et al., 2007).

3.2. Cesium

The radiography technique measures the change in X-ray absorption as a function of the mass of Cs^+ in the X-ray path, and the relative concentrations presented in Fig. 4 represent Cs^+ in the pore solution and on exchange sites. As a result, the relative concentrations exceed unity near the boundary as Cs^+ mass increases in the pore fluid and additional Cs^+ accumulates on the exchange sites (Fig. 4a).

The experimental Cs^+ profiles cannot be fit with diffusion-only (no sorption) simulations (Fig. 4a) as was done for I^-, but a good fit is obtained with the model that couples diffusion and

single-site cation exchange (Fig. 4b). The approach taken here is simpler than the Cs^+ sorption models used in several other investigations which employ either a two-site (Liu et al., 2004; Melkior et al., 2005) or more commonly, a three-site model to describe the uptake of Cs^+ at much lower concentrations, ≤0.001 mol/L Cs^+ (Bradbury and Baeyens, 2000; Maes et al., 2008; Steefel et al., 2003; van Loon et al., 2009). The three-site model for Cs^+ adsorption on illite (Bradbury and Baeyens, 2000), identifies the sites in order of decreasing selectivity as frayed-edge sites (FES), type II sites and planar sites. Generally, it is thought that the FES dominate Cs^+ sorption at concentrations $<10^{-8}$ mol/L Cs^+, type II sites become dominant between 10^{-8} to 10^{-5} mol/L and planar sites dominate sorption at Cs^+ concentrations $>10^{-3}$ mol/L (Jakob et al., 2009). However, the effective ranges of Cs^+ concentration for the different exchange sites would also vary with mineralogy and CEC. The single-site approach used in this work is consistent with the Bradbury and Baeyens (2000) three site model because the high Cs^+ concentration in this work would be expected to mask any influence from the FES and type II sites on the selectivity coefficient.

The PEST code provides an indication of the degree of parameter correlation when fitting multiple parameters simultaneously. A moderate degree of correlation was indicated between $D_{p\text{-}Cs}$ and log $K_{Cs+/Na+}$ (correlation coefficients for the three samples ranged from -0.59 to -0.61) and $D_{p\text{-}Cs}$ and CEC (correlation coefficient range 0.55 to 0.56), but a high degree of correlation was indicated between log $K_{Cs+/Na+}$ and CEC (correlation coefficient range -0.94 to -0.95). To further investigate parameter correlation, PEST was used to fit two parameters simultaneously while holding one parameter constant. When fitting $D_{p\text{-}Cs}$ to either log $K_{Cs+/Na+}$ or CEC, the correlation dropped in magnitude to 0.0 – 0.3, indicating that $D_{p\text{-}Cs}$ is, in fact, independent of log $K_{Cs+/Na+}$ and CEC. However, while holding $D_{p\text{-}Cs}$ constant, the correlation coefficient between

log $K_{Cs+/Na+}$ and CEC does not decrease. To test the independence of these two variables, PEST was used repeatedly to find the best fit while changing the initial values to force convergence from different directions (Poeter and Hill, 1998). Parameters for samples D and F were estimated an additional five times with the initial values ranging from 0.5 to 5.0 (log $K_{Cs+/Na+}$), 2.0 to 20 meq/100 g (CEC), and 2.0 x10^{-11} to 6.0 x 10^{-10} m^2/s (D_{p-Cs}). In all cases, the best-fit parameter values fell within the 95% confidence intervals determined for the initial estimations (Table 4). These results indicate that the correlation between log $K_{Cs+/Na+}$ and CEC is still low enough to provide a unique estimation for all three parameters.

The estimates of D_{p-Cs}, log $K_{Cs+/Na+}$ and CEC from triplicate analyses demonstrate good agreement (Table 4). Pore diffusion coefficients for Cs^+ (mean of 7.6 x10^{-11} m^2/s) are double the D_{p-I} values (mean of 3.8 x10^{-11} m^2/s; Table 4) and are also higher than the D_{p-HTO} value of 5.3 x 10^{-11} m^2/s measured with tritiated-water tracer (HTO) in similar Queenston Formation shale by through-diffusion (Al et al., 2010). The relatively high Cs^+ diffusion coefficients commonly reported in the literature are typically attributed to preferential transport through clay interlayers and/or externally bound double-layer water (Altmann et al., 2012; Appelo et al., 2010; Jakob et al., 2009; Melkior et al., 2007; Tachi et al., 2011; Wersin et al., 2008). The overall transport rate, however, for the cation species Cs^+ is slower than for conservative tracers because of sorption effects (Fig. 4a). The D_{p-Cs} values from this study are approximately two orders of magnitude lower than the D_{p-Cs} values reported from European and Japanese argillaceous sediments (Table 4). This magnitude of difference is consistent with the low diffusion coefficients measured in the Queenston Formation shale using other tracers (I^- and HTO) (Al et al., 2010, 2012; Cavé et al., 2009; Mazurek et al., 2008; Tachi et al., 2011; Xiang et al., in press) and are attributable to the lower bulk porosity of the Michigan Basin shale (Table 4).

The mean log $K_{Cs+/Na+}$ value of 1.5 is very close to the value of 1.6 determined by Bradbury and Baeyens (2000) for planar sites on illite (Table 4). Other reported values for log $K_{Cs+/Na+}$ on various exchange sites tend to be higher (Table 4), but increasing log $K_{Cs+/Na+}$ to 2.0 or greater produces a steepening of the simulated profiles that is not observed in the experimental data (Fig. 5a). Similarly, lower values for log $K_{Cs+/Na+}$, such as the value of 1.097 for soil reported by Appelo and Postma (2005), reduces the curvature of the simulated profile and does not fit well with the experimental data (Fig. 5a).

The mean CEC value of 8.4 ±0.3 meq/100 g is lower than the CEC value of 12.5 reported by Barone et al. (1990) for disaggregated Queenston shale from a shallow drill core containing low salinity porewater. In this work, inclusion of CEC values greater than 8.4 meq/100 g in the simulations leads to overestimation of the relative Cs^+ concentration at the influx boundary and a slight over-steepening of the profile (Fig. 5b). Natural variation in mineralogy of Queenston Formation shale (Table 1), and variations in porewater salinity may account for the difference between the CEC reported by Barone et al. (1990) and that obtained by the present experiments. Cation exchange capacity values for other argillaceous formations that are under consideration for radioactive waste disposal are relatively high but also variable within formations (9.5-25 meq/100 g; Table 4).

It is not possible to measure the Cs^+-accessible porosity in a manner similar to the determination of ϕ. Instead, the quantification of relative Cs^+ concentrations relies on a calibration curve, with the $\Delta\mu$ measurements scaled by ϕ_w (Equation 6). For the diffusion-reaction experiment, it is assumed that there are no ion exclusion effects and that 100% of the water-accessible porosity is also accessible to Cs^+. Other studies have applied the HTO-accessible

porosity, ϕ_{HTO}, to the Cs^+ cation (e.g., Maes et al., 2008). Small differences in porosity can lead to significant differences in the calculated C/C_0 values. Porosity is also used as a scaling parameter when converting between D_p and D_e. Thus, it is important to evaluate the sensitivity of the results to variations in the measured porosity.

The diffusion-reaction modeling was performed by adjusting the value of porosity by ±10% (0.098 and 0.120) and determining the best-fit parameter values. Decreasing the porosity by 10% results in an increase in CEC of 9%, an increase in log $K_{Cs+/Na+}$ of 0.6%, and a decrease in $D_{p\text{-}Cs}$ of 0.1%. Increasing the porosity by 10% results in changes of similar magnitude but opposite sign for the fitted parameters. These results demonstrate that the estimations of log $K_{Cs+/Na+}$ and $D_{p\text{-}Cs}$ are insensitive to porosity, but the estimation of CEC is quite sensitive to porosity. Surface reactions are dependent on the solid to liquid ratio which accounts for the sensitivity of CEC to porosity. Given the method sensitivity to porosity and the natural variations in porosity –a range of 0.078 - 0.109 has been measured in the Queenston Formation shale (Table 1) –bulk porosities should be measured from sub-samples of the same material used for the diffusion experiments as opposed to using a generic average porosity for a Formation.

4. Conclusions

An X-ray radiography method has been applied to the estimation of diffusion-reaction parameters for Cs^+ transport in low permeability sedimentary rock. Cesium transport was monitored non-destructively to obtain time- and space-resolved profiles of relative Cs^+ concentrations during diffusion-reaction experiments. Data is extracted from the transient period of transport, and therefore, meaningful results were available within days of the start of the experiments.

A single-site ion exchange model that coupled diffusion and ion-exchange was used successfully to simulate the time-series profiles by fitting three parameters simultaneously: $D_{p\text{-}Cs}$, log $K_{Cs+/Na+}$ and the CEC. The measured $D_{p\text{-}Cs}$ was lower than values reported for other argillaceous formations. However, the low $D_{p\text{-}Cs}$ is consistent with low diffusion coefficients for other tracers in Queenston Formation shale, and the relative magnitudes of the diffusion coefficients ($D_{p\text{-}I} < D_{p\text{-}HTO} < D_{p\text{-}Cs}$) are consistent with findings from other studies. The D_p parameter is independent of tracer concentration and solution composition and therefore, values determined by this method will be representative over a range of concentrations relevant to engineered barriers and host rocks for radioactive waste repositories.

Despite the correlation between log $K_{Cs+/Na+}$ and CEC, it was possible to obtain a unique estimation for all three parameters. This method of determining CEC avoids the problems of high porewater salinity that confound CEC measurements by common batch sorption experiments, and given that CEC is independent of tracer concentration, these CEC values are also applicable to the range of Cs concentrations expected in engineered barriers and host rocks to radioactive waste repositories. The selectivity coefficient determined for Cs^+ using this approach is consistent with the literature values of log $K_{Cs+/Na+}$ for Cs^+ sorption dominated by planar sites. Future research will determine whether selectivity coefficients can be determined by this method for exchange sites that are relevant at much lower Cs concentrations using a multi-site sorption model.

Acknowledgements

This work was supported by funding from the Nuclear Waste Management Organization (NWMO). Technical support was provided by the Microscopy and Microanalysis Facility, University of New Brunswick.

References

Al, T., Xiang, Y., Cavé, L., 2010. Measurement of Diffusion Properties by X-ray Radiography and by Through-Diffusion Techniques Using Iodide and Tritium Tracers: Core Samples from OS-1 and DGR-2. TR-07-17 Revision 3. Report prepared for Intera Engineering Ltd. (now Geofirma Engineering Ltd.), May 19, 2010. Report available online through http://www.nwmo.ca.

Al, T., Xiang, Y., Cavé, L., Loomer, D., 2012. Measurement of Diffusion Properties by X-Ray Radiography and by Through-Diffusion Techniques Using Iodide and Tritium Tracers: Core Samples from DGR-3 and DGR-4. TR-08-27 Revision 2, May 2012. Report prepared for Geofirma Engineering Ltd., June, 2012. Report available online through http://www.nwmo.ca.

Aldaba, D., Rigol, A., Vidal, M., 2010. Diffusion experiments for estimating radiocesium and radiostrontium sorption in unsaturated soils from Spain: Comparison with batch sorption data. J. Hazard. Mater. 181, 1072–1079.

Altmann, S., Tournassat, C., Goutelard, F., Parneix, J.-C., Gimmi, T., Maes, N., 2012. Diffusion-driven transport in clayrock formations. Appl. Geochem. 27, 463–478.

André, M., Malmström, M.E., Neretnieks, I., 2009. Determination of sorption properties of intact rock samples: New methods based on electromigration. J. Contam. Hydrol. 103, 71–81.

Appelo, C., Postma, D., 1993. Geochemistry, Groundwater and Pollution. A.A. Balkema Publishers, Rotterdam, 526 p.

Appelo, C.A.J., Postma, D., 2005. Geochemistry, Groundwater and Pollution, second ed. A.A. Balkema, Amsterdam.

Appelo, C.A.J., van Loon, L.R., Wersin, P., 2010. Multicomponent diffusion of a suite of tracers (HTO, Cl, Br, I, Na, Sr, Cs) in a single sample of Opalinus Clay. Geochim. Cosmochim. Acta 74, 1201–1219.

Barone, F.S., Rowe, R.K., Quigley, R.M., 1990. Laboratory determination of chloride diffusion coefficient in an intact shale. Can. Geotech. J. 27, 177–184.

Bea, S.A., Carrera, J., Ayora, C., Batlle, F., 2010. Pitzer Algortithm: Efficient implementation of Pitzer equations in geochemical and reactive transport models. Comput. Geosci. 36, 526–538.

Bea, S.A., Mayer, K.U., MacQuarrie, K.T.B., 2011. Modelling Reactive Transport in Sedimentary Rock Environments - Phase II, MIN3P code enhancements and illustrative simulations for a glaciation scenario. Nuclear Waste Management Organization, Toronto,

ON, Technical report NWMO TR-2011-13. Report available online through http://www.nwmo.ca.

Bradbury, M.H., Baeyens, B., 1998. A physicochemical characterisation and geochemical modeling approach for determining porewater chemistries in argillaceous rocks. Geochim. Cosmochim. Acta 62, 783–795.

Bradbury, M.H., Baeyens, B., 2000. A generalized sorption model for the concentration dependent uptake of caesium by argillaceous rocks. J. Contam. Hydrol. 42, 141–163.

Bazer-Bachi, F., Tevissen, E., Descostes, M., Grenut, B., Meier, P., Simonnot, M.-O., Sardin, M., 2006. Characterization of iodide retention on Callovo-Oxfordian argillites and its influence on iodide migration. Phys. Chem. Earth, 31, 517–522.

Briscoe, G., Wigston, A., Melaney, M., 2010. Drilling, Logging and Sampling of DGR-3 and DGR-4. Technical Report TR-08-13 Revision 0, February 2010. Prepared by Intera Engineering Ltd. (now Geofirma Engineering Ltd.) for the NWMO. Report available online through http://www.nwmo.ca.

Cavé, L., Al, T., Xiang, Y., Vilks, P., 2009. A technique for estimating one-dimensional diffusion coefficients in low permeability sedimentary rock using X-ray radiography: Comparison with through-diffusion measurements. J. Contam. Hydrol. 103, 1–12.

Cormenzana, J.L, García-Gutiérrez, M., Missana, T., Junghanns, Á., 2003. Simultaneous estimation of effective and apparent diffusion coefficients in compacted bentonite. J. Contam. Hydrol. 61, 63–72.

Doherty, J., 2010. Open-source model-independent parameter estimation and uncertainty analysis software - PEST. Version 12.2. Available at http://www.pesthomepage.org/.

García-Gutiérrez, M., Cormenzana, J.L., Missana, T., Alonso, U., Mingarro, M., 2011. Diffusion of strongly sorbing cations (^{60}Co and ^{152}Eu) in compacted FEBEX bentonite. Phys. Chem. Earth 36, 1708–1713.

Harvie, C.E. Moller, N., Weare, J.H., 1984. The prediction of mineral solubilities in natural waters: The Na-K-Mg-Ca-H-Cl-SO_4-OH-HCO_3-CO_3-CO_2-H_2O system to high ionic strengths at 25^{o}C. Geochim. Cosmochim. Acta 48, 723–751.

Jackson, R., 2009. Organic Geochemistry and Clay Mineralogy of DGR-3 and DGR-4 Core, Revision 0. TR-08-29. Report prepared for Intera Engineering Ltd., November, 2009. Report available online through http://www.nwmo.ca.

Jakob, A., Pfingsten, W., van Loon, L., 2009. Effects of sorption competition on cesium diffusion through compacted argillaceous rock. Geochim. Cosmochim. Acta 73, 2441–2456.

Koroleva, M., de Haller, A., Mader, U., Waber, H.N., Mazurek, M., 2009. Borehole DGR-2: Pore-Water Investigations, Revision 0. TR-08-06. Report prepared for Intera Engineering Ltd. (now Geofirma Engineering Ltd.), August, 2009. Report available online through http://www.nwmo.ca.

Liu, C., Zachara, J.M., Smith, S.C., 2004. A cation exchange model to describe Cs^+ sorption at high ionic strength in the subsurface sediments at Hanford site, USA. J. Contam. Hydrol. 68, 217–238.

Lutus, P. 2011. PolySolve Version 3.4 (02-27-2011). Polynomial Regression Data Fit java applet. Available at http://www.arachnoid.com/polysolve/index.html.

Maes, N., Salah, S., Jacques, D., Aertsens, M., van Gompel, M., de Cannière, P., Velitchkova, N., 2008. Retention of Cs^+ in Boom Clay: Comparison of data from batch sorption and diffusion experiments on intact clay cores. Phys. Chem. Earth 33, S149–S155.

Mayer, K.U., Frind, E.O., Blowes, D.W., 2002. Multicomponent reactive transport modeling in variably saturated porous media using a generalized formulation for kinetically controlled reactions. Water Resour. Res. 38, 1174–1194.

Mazurek, M., Gautschi, A., Marschall, P., Vigneron, G., Lebon, P., Delay, J., 2008. Transferability of geoscientific information from various sources (study sites, underground rock laboratories, natural analogues) to support safety cases for radioactive waste repositories in argillaceous formations. Phys. Chem. Earth 33, S95–S105.

Melkior, T., Mourzagh, D., Yahiaoui, S., Thoby, D., Alberto, J.C., Brouard, C., Michau, N., 2004. Diffusion of an alkaline fluid through clayey barriers and its effect on the diffusion properties of some chemical species. Appl. Clay Sci. 26, 99– 107

Melkior, T., Yahiaoui, S., Motellier, S., Thoby, D., Tevissen, E., 2005. Cesium sorption and diffusion in Bure mudrock samples. Appl. Clay Sci. 29, 172–186.

Melkior, T., Yahiaoui, S., Thoby, D., Motellier, S., Barthès, V., 2007. Diffusion coefficients of alkaline cations in Bure mudrock. Phys. Chem. Earth 32, 453–462.

Okuyama, K., Sasahira, A., Noshita, K., Ohe, T., 2008. A method for determining both diffusion and sorption coefficients of rock medium within a few days by adopting a micro-reactor technique. Appl. Geochem. 23, 2130–2136.

Pinder, L., 2009. Drilling Fluid Management and Testing in DGR-3 and DGR-4. Technical Report TR-08-16 Revision 0, November 2009. Prepared by Intera Engineering Ltd. (now Geofirma Engineering Ltd.) for OPG. Report available online through http://www.nwmo.ca.

Pitzer, K.S., Mayorga, G., 1973. Thermodynamics of electrolytes. 2. Activity and osmotic coefficients for strong electrolytes with one or both ions univalent. J. Phys. Chem.-US 77, 2300–2308.

Pitzer, K.S., Kim, J.J., 1974. Thermodynamics of electrolytes. 4. Activity and osmotic coefficients for mixed electrolytes. J. Am. Chem. Soc. 96, 5701–5707.

Pearson, F.J., Arcos, D., Bath, A., Boisson, J.-Y., Fernández, A.M., Gäbler, H.-E., Gaucher, E., Gautschi, A., Griffault, L., Hernán, P., Waber, H.N., 2003. Mont Terri Project – Geochemistry of Water in the Opalinus Clay Formation at the Mont Terri Rock Laboratory. Reports of the Swiss Federal Office for Water and Geology (FOWG), Geology Series No. 5, 319 p.

Poeter, E.P. and Hill, M.C., 1998. Documentation of UCODE, A Computer Code for Universal Inverse Modeling. U.S. Geological Survey Water-Resources Investigations Report 98-4080, Denver, Colorado.

Rasband, W.S., 2012. ImageJ, U. S. National Institutes of Health, Bethesda, Maryland, USA, http://imagej.nih.gov/ij/, 1997-2012.

Reardon, E.J., 1981. K_d's — Can They Be Used to Describe Reversible Ion Sorption Reactions in Contaminant Migration? Groundwater 19, 279–286.

Soler, J.M., Wersin, P., Leupin, O., 2013. Modeling of Cs^+ diffusion and retention in the DI-A2 experiment (Mont Terri). Uncertainties in sorption and diffusion parameters. Appl. Geochem. 33, 191-198.

Staunton, S. and Roubaud, M., 1997. Adsorption of ^{137}Cs on montmorillonite and illite: Effect of charge compensating cation, ionic strength and concentration of Cs, K, and fulvic acid. Clays Clay Miner. 45, 251–260.

Steefel, C.I., Carroll, S., Zhao, P., Roberts, S., 2003. Cesium migration in Hanford sediment: a multisite cation exchange model based on laboratory transport experiments. J. Contam. Hydrol. 67, 219– 246.

Tachi, Y., Yotsuji, K., Seida, Y., Yui, M., 2011. Diffusion and sorption of Cs+, I_ and HTO in samples of the argillaceous Wakkanai Formation from the Horonobe URL, Japan: Clay-based modeling approach. Geochim. Cosmochim. Acta 75, 6742–6759.

van Loon, L.R., Baeyens, B., Bradbury, M.H., 2005. Diffusion and retention of sodium and strontium in Opalinus clay: Comparison of sorption data from diffusion and batch sorption measurements, and geochemical calculations. Appl. Geochem. 20, 2351–2363.

van Loon, L.R., Baeyens, B., Bradbury, M.H., 2009. The sorption behaviour of caesium on Opalinus clay: A comparison between intact and crushed material. Appl. Geochem. 24, 999–1004.

van Loon, L.R., Glaus, M.A., Muller W., 2007. Anion exclusion effects in compacted bentonites: Towards a better understanding of anion diffusion. Appl. Geochem. 22, 2536-2552.

Wersin, P., Soler, J.M., van Loon, L., Eikenberg, J., Baeyens, B., Grolimund, D., Gimmi, T., Dewonck, S., 2008. Diffusion of HTO, Br^-, I^-, Cs^+, $^{85}Sr^{2+}$ and $^{60}Co^{2+}$ in a clay formation: Results and modelling from an in situ experiment in Opalinus Clay. Appl. Geochem. 23, 678–691.

Wildenschild, D., Hopmans, J.W., Vaz, C.M.P., Rivers, M.L., Rikard, D., 2002. Using X-ray computed tomography in hydrology: Systems, resolutions, and limitations, J. Hydrol. 267, 285–297.

Xiang, Y., Al, T., Scott, L., Loomer, D., in press. Diffusive anisotropy in low-permeability Ordovician sedimentary rocks from the Michigan Basin in southwest Ontario. Manuscript accepted for publication in J. Contam. Hydrol.

Zachara, J.M., Smith, S.C., Liu, C., McKinley, J.P., Serne, R.J., Gassman, P.L, 2002. Sorption of Cs to micaceous subsurface sediments from the Hanford site, USA. Geochim. Cosmochim. Acta 66, 193–211.

Table 1

Water-accessible porosity and mineralogy of red shale samples from the Queenston Formation.

Sample	Mean ϕ_w [a]		Reference	
DGR2-456.97	0.090 ± 0.005		Al et al. 2010	
DGR2-517.96	0.078 ± 0.003		Al et al. 2010	
DGR3-468.02	0.109		Al et al. 2012	
DGR4-516.89	0.093		Al et al. 2012	
Mineralogy [b]	DGR2 [c]	DGR3-521.05 [d]	DGR4-468.92 [d]	DGR4-514.92 [d]
Quartz	4-12	23.5	18.5	34.1
K-feldspar	<2	1.4	1.3	3.2
Plagioclase	<2	1.2	1.9	1.9
Calcite	8-57	14.6	31.6	6.1
Dolomite/ankerite	7-31	6.6	7.6	11.4
Clay minerals	29-53	45.2	36.6	41.0
Illite/mica [e]	-	*60.9*	*60.1*	*58.2*
Illite/smectite [e]	20-39	-	*11.9* [f]	*9.7* [f]
Chlorite [e]	9-14	*39.1*	*24.5*	*29.1*
Kaolinite [e]	<1	-	*3.5*	*3.0*
Pyrite	-	-	0.5	-
Hematite	-	7.5	2.1	2.2
Organic C	<0.1-0.3	0.073	0.13	0.12

[a] Measured after drying subsamples to a constant mass at 105 ˚C

[b] In units of wt%

[c] Koroleva et al. (2009); [d] Jackson (2009)

[e] Values in italic are expressed as wt% of the clay fraction.

[f] Mixed-layer illite/smectite contains 5-10% smectite layers.

Table 2

Composition (mol/L) of solutions used in porosity measurements and diffusion experiments.

	SPW	I^- Tracer	Cs^+ Tracer
Na^+	2.4	2.4	1.4
K^+	0.5	0.5	0.5
Ca^{2+}	1.2	1.2	1.2
Mg^{2+}	0.25	0.25	0.25
Cl^-	5.8	4.8	5.8
SO_4^{2-}	0.001	0.001	0.001
I^-	-	1.0	-
Cs^+	-	-	1.0

Table 3

Binary and ternary virial coefficients for Cs^+ added to the database for the MIN3P simulations.

Binary coefficients:					
Ion-pair	B_0	B_1	C_0	θ	Reference
Cs^+ Cl^-	0.030	0.0558	0.00038		Pitzer and Mayorga, 1973
Cs^+ SO_4^{2-}	0.0888	1.11075	0.00004		
Cs^+ OH^-	0.150	0.30	-0.00599803		
Cs^+ Na^+				-0.033	Pitzer and Kim, 1974
Cs^+ K^+				0.0	
Cs^+ H^+				-0.044	

Ternary coefficients:		
Ion group	ψ	Reference
Cs^+ Na^+ Cl^-	-0.003	Pitzer and Kim, 1974
Cs^+ K^+ Cl^-	-0.0013	
Cs^+ H^+ Cl^-	-0.019	

Cs^+-Mg^{2+}, Cs^+-Ca^{2+} coefficients and SO_4^{2-} ternary coefficients were not included in the database because published values could not be shown to be consistent with the parameters listed here.

Table 4

Diffusion results for I^-, diffusion-sorption results for Cs^+ and comparison with other studies.

This Study	Ionic strength	ϕ	C_0 I^- (mol/L)		$D_{p\text{-}I}$ ($x10^{-11}$ m^2/s)	$D_{e\text{-}I}$ ($x10^{-11}$ m^2/s)				
Queenston shale A [a]	8.3	0.078	10^0	⊥	4.3±0.6	0.34				
Queenston shale B [a]		0.078		⊥	4.5±0.2	0.35				
Queenston shale C [a]		0.072		⊥	2.6±0.1	0.19				
	Ionic strength	ϕ	C_0 Cs^+ (mol/L)		$D_{p\text{-}Cs}$ [d] ($x10^{-11}$ m^2/s)	$D_{e\text{-}Cs}$ [d] ($x10^{-11}$ m^2/s)	Exchange site(s)	log $K_{Cs+/Na+}$	CEC (meq/100g)	Clay (wt%)
Queenston shale D [b]	8.4	0.109	10^0	⊥	7.7 ± 0.08	0.84	X	1.5 ± 0.04	8.5 ± 0.3	40-50
Queenston shale E [b]				⊥	7.7 ± 0.03	0.84		1.5 ± 0.01	8.7 ± 0.1	
Queenston shale F [b]				⊥	7.4 ± 0.04	0.81		1.6 ± 0.02	8.0 ± 0.2	
Queenston Mean ± σ [c]				⊥	7.6 ± 0.17	0.83		1.5 ± 0.03	8.4 ± 0.3	
Hanford sediments [e]	5	-	10^{-10} – 10^{-1}		-	-	Site I Site II	7.2 2.3	8.25	2.7
Hanford sediments [f]	0.1 - 5	0.40	10^{-7} – 10^{-4}		-	-	FES 1 (0.02% of CEC) FES 2 (0.22% of CEC) Planar (99.8% of CEC)	7.25 4.93 1.99	12	2.7
Bure mudrock [g]	0.05	0.14	10^{-9} – 10^{-2}	⊥	160-190	23-27	Weak Strong	4.6 (Cs^+/Ca^{2+})	14 – 21	24–50
Reference illite [h]	≤ 0.1	-	10^{-10} – 10^{-3}		-	-	FES (0.25% of CEC) Type II (20% of CEC) Planar (80% of CEC)	7 3.6 1.6	20	-
Opalinus Clay at Mont Terri	0.4	0.15-0.18 [i]	10^{-3}	∥	130-170 [i]	20-30 [i]	FES (0.06% of CEC)	7.1[k]/7.0 [n]	10-11 [l]	54–76 [l,m]
		0.16 [j]		⊥	110 [j]	18 [j]	Type II (0.6% of CEC)	4.6 [k]/3.2 [n]	9.45-16.9 [m]	
		0.16 [k]		∥	132 [k]	21 [k]	Planar (≈CEC)	2.0 [k]/1.6 [n]	12.74 [k]	
		0.154 [n]		∥	130-260 [n]	20-40 [n]			9.5 [n]	
Boom clay [o]	0.02	0.37	10^{-9} – 10^{-2}	⊥	380	140	FES	7	~ 25	30–60
Wakkanai Fm [p]	0.02-0.7	0.37	10^{-5}	∥∥	73-410	27-150	FES/Type II/Planar	-	20	27
Soil exchange coeff. [q]	-	-	-		-	-	X	1.097	-	-
FEBEX bentonite	-	-	-		-	3-10 [r]	-	-	102 ± 4 [r]	93 ± 2 [s]

⊥ ∥ ∥∥ indicate the orientation of the measurements relative to sample bedding as normal, parallel and inclined 45°, respectively.

[a] The ± values represent 1σ from the mean of multiple time series; [b] The ± values represent 95% confidence limits determined through PEST; [c] σ = standard deviation about the mean; [d] When required, the conversion between D_p and D_e has been made based on $D_e = D_p \cdot \varphi$. [e] Liu et al., 2004; [f] Steefel et al., 2003; [g] Melkior et al., 2005; [h] Bradbury and Baeyens, 2000; [i] Wersin et al., 2008; [j] Jakob et al., 2009; [k] Appelo et al., 2010; [l] Mazurek et al., 2008 (listed as representative); [m] Pearson et al., 2003 (range measured by various methods); [n] Soler et al., 2013, determined parallel to bedding; [o] Maes et al., 2008; [p] Tachi et al., 2011; [q] Appelo and Postma, 2005; [r] Cormenzana et al., 2003; [s] García-Gutiérrez et al., 2011.

Fig. 1. Diagram of the cell used for diffusion experiments by X-ray radiography.

Fig. 2. Calibration curves developed for (a) I^- and (b) Cs^+; (○) glass vial calibration; (△) ceramic vials; (×) sandstones. The sandstone calibration curve was used for the ϕ_I measurements. The sandstone equivalent calibration curve used to determine the mass of Cs^+ in the diffusion samples (dashed line in b) is based on the relative differences observed between the calibration matrices for I^- and Cs^+. Error bars represent 1σ.

Fig. 3. Iodide-diffusion time-series profiles and iodide-accessible porosity (dotted line) for sample B. The solid lines represent the fit to the experimental data for each profile in the time series.

Fig. 4. Diffusion-reaction time-series profiles for Queenston shale sample F: (a) compares experimental Cs^+ diffusion-reaction profiles (symbols) with simulated diffusion profiles for corresponding times; (b) illustrates the best fit simulated Cs^+ diffusion-reaction profiles (lines) with the same experimental data (symbols).

Fig. 5. Sensitivity analysis for individual parameters in the reactive transport model: (a) log $K_{Cs+/Na+}$, dimensionless, (b) CEC in units of meq/100 g and (c) $D_{p\text{-}Cs}$ in units of m^2/s. The profiles represent 5.7 days total diffusion-reaction time for sample F.

Highlights

- X-ray radiography was used to determine Cs transport parameters in intact rock.
- Reactive-transport modeling was used to simultaneously estimate 3 parameters.
- $D_{p\text{-}Cs} = 7.6 \times 10^{-11}$ m^2/s, log $K_{Cs+/Na+} = 1.5$ and CEC = 8.4 meq/100 g in shale.

Fig1

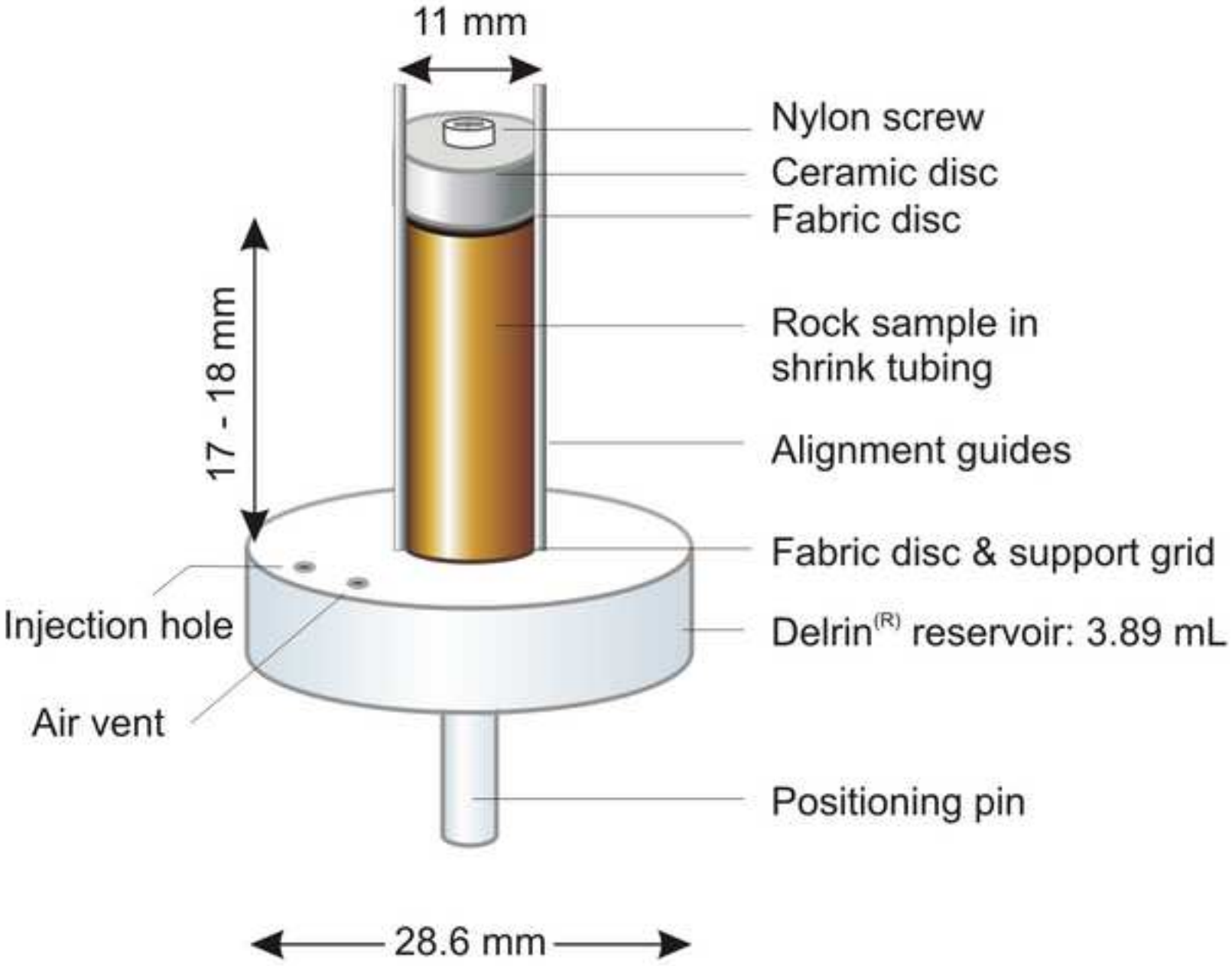

Fig2

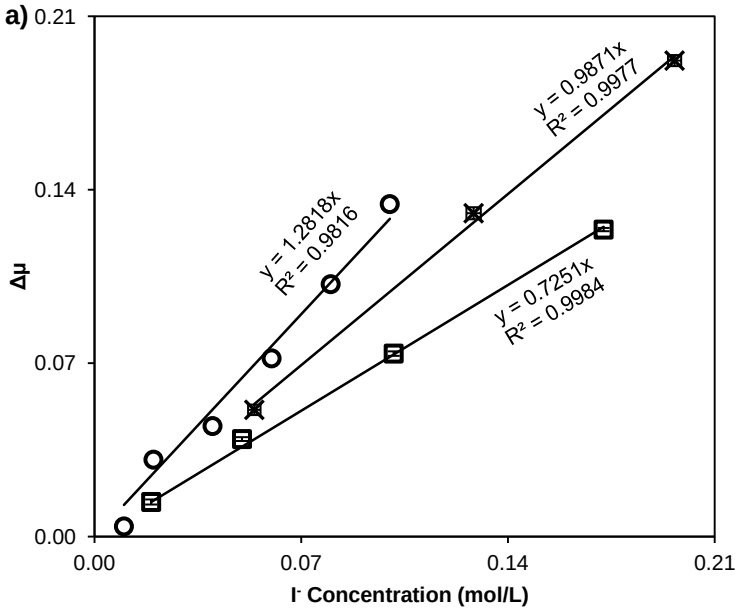

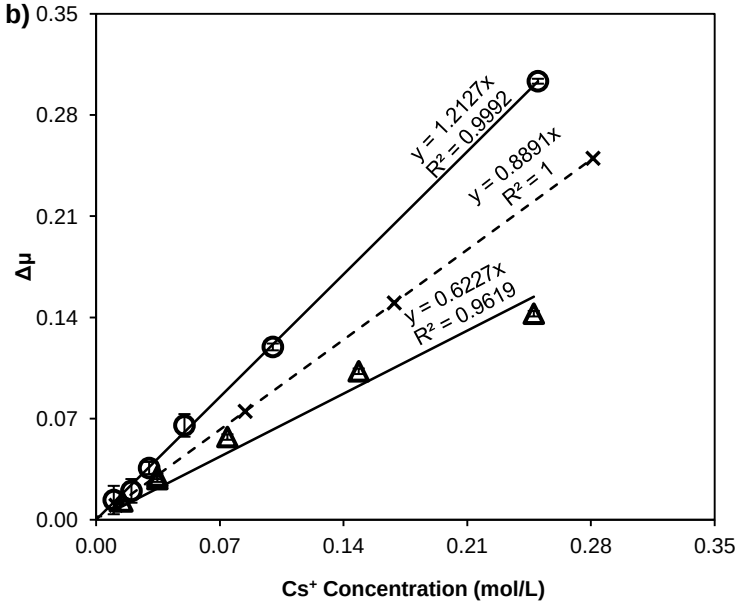

Fig3

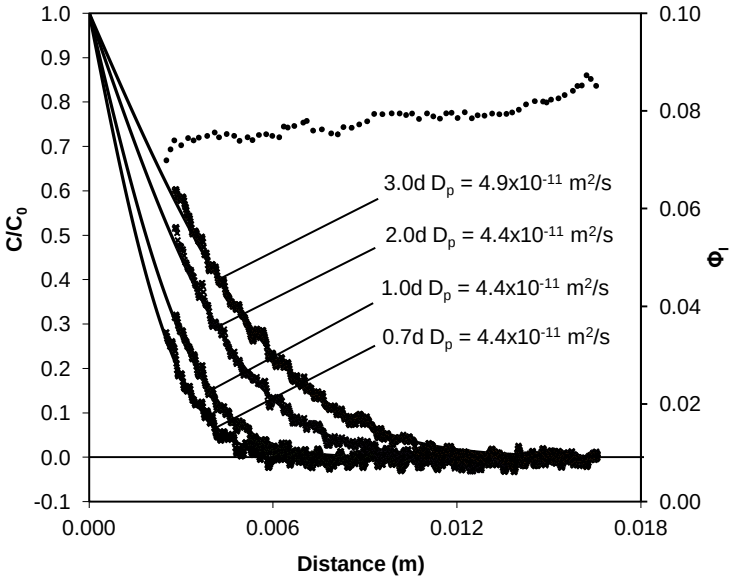

Fig4

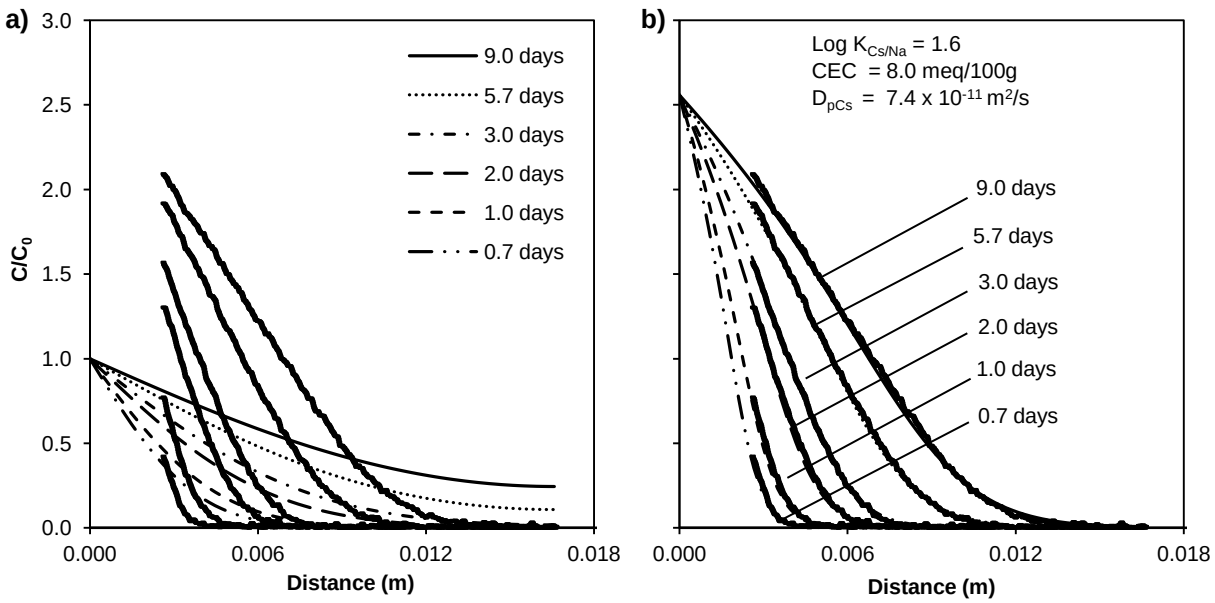

Fig5

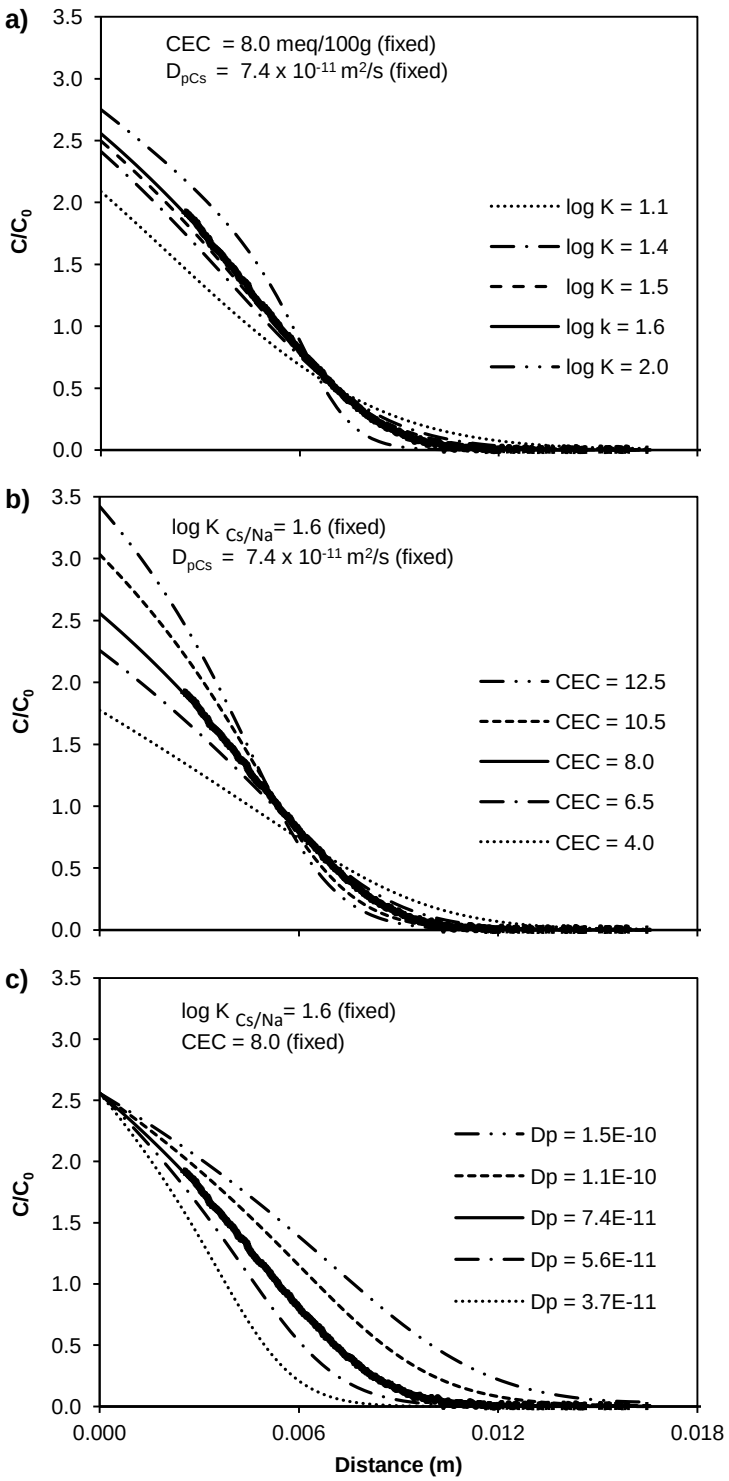

graphic_abstract